JOURNAL OF GEOPHYSICAL RESEARCH, VOL. 113, B08409, doi:10.1029/2007JB005538, 2008



# Time dependence in 3-D mantle convection models featuring evolving plates: Effect of lower mantle viscosity

A. D. Gait,[1,2] J. P. Lowman,[3,4] and C. W. Gable[5]

Received 3 December 2007; revised 7 May 2008; accepted 3 June 2008; published 19 August 2008.

[1] Evolving plate configurations and dynamically determined plate velocities are featured in Cartesian geometry mantle convection simulations. The numerical model enables the evolution of plate shape and size by migrating idealized plate triple junctions. The motion of the model triple junctions responds to the time-dependent velocities of the adjacent plates. Each calculation includes four high-viscosity plates in a $3 \times 3 \times 1$ solution domain. We analyze the effect of plate evolution on the time dependence of plate velocity and heat flux in three different models characterized by lower mantle to upper mantle viscosity ratios of 30, 90, and 300. We examine the difference in behavior between calculations featuring fixed and mobile plate boundaries for each viscosity model. When plates are permitted to evolve in response to the convective vigor of the system, plate positions and shapes can change considerably while features in the high-viscosity lower mantle may change very little. In addition, plate velocities and surface heat flux can be highly time dependent. We find that when the contrast between lower mantle and upper mantle viscosity magnitude is a factor of 30, surface velocities may fluctuate by 75% of the mean value and heat flux by 60%. We also find that plate velocity evolution is characterized by periods of reorganization, punctuating more stable periods. When the lower mantle viscosity is increased to 90 times the upper mantle value, plate reorganization events also occur, but only when plate boundary motion is enabled. When the lower mantle to upper mantle viscosity contrast is increased to a factor of 300, we find that the mean surface velocity and heat flux become very steady in cases both with and without plate boundary evolution, despite the substantial migration of convergent plate boundaries in the former case.

**Citation:** Gait, A. D., J. P. Lowman, and C. W. Gable (2008), Time dependence in 3-D mantle convection models featuring evolving plates: Effect of lower mantle viscosity, *J. Geophys. Res.*, *113*, B08409, doi:10.1029/2007JB005538.

## 1. Introduction

[2] The motion of the Earth's tectonic plates is an expression of the vigorous convection in its interior. To simplify the description of the instantaneous motion of the Earth's surface it is possible to separate the movement into components, namely, the uniform rigid body velocity of the individual plates [e.g., *Minster and Jordan*, 1978; *Gordon et al.*, 1978; *DeMets et al.*, 1990, 1994] and the motion of the plate boundaries, which causes the plates to change size and shape. The peculiarity of plate-like motion, in comparison to the surface motion obtained in most convecting systems, has been widely described [*Tackley*, 1998, 2000a, 2000b, 2000c; *Trompert and Hansen*, 1998; *Bercovici*, 2003]. Piecewise uniform surface velocity is not typically obtained from a viscous convecting fluid [e.g., *Solomatov and Moresi*, 1997; *Richards et al.*, 2001; *Stein et al.*, 2004], yet plate-like surface motion is a requirement if a model of terrestrial mantle convection is to be considered realistic [*Bercovici*, 2003]. Moreover, if the goal is to model a system that features realistic plate evolution then time-dependent plate velocities as well as motion of the boundaries outlining the plates must both be present [*Zhong and Gurnis*, 1995].

[3] Plate boundary velocities are comparable to the velocities of the plates themselves. Consequently, if plate velocities are representative of mantle velocities, plates can be drastically reshaped in a single mantle transit time [*Bercovici*, 2003]. As long as some plate boundaries migrate, the plate morphologies will evolve at a rate that is significant compared to the velocities in the mantle. For example, the Atlantic has formed in roughly the same amount of time that a subducted parcel of material descending at an average velocity of 2 cm/a (where a is years) will have taken to reach the core mantle boundary. The mid-Atlantic ridge has not migrated significantly in this time

[1]School of Earth and Environment, University of Leeds, Leeds, UK.
[2]Now at School of Mathematics, University of Manchester, Manchester, UK.
[3]Department of Physical and Environmental Sciences, University of Toronto Scarborough, Toronto, Ontario, Canada.
[4]Also at Department of Physics, University of Toronto, Toronto, Canada.
[5]Hydrology, Geochemistry, and Geology Group, EES-6, Los Alamos National Laboratory, Los Alamos, New Mexico, USA.


0148-0227/08/2007JB005538$09.00

although the adjacent plates have changed their dimensions considerably. Mantle convection studies featuring nonevolving plate boundaries are limited in their ability to capture realistic rates of system time dependence and may exaggerate the coupling between plate boundaries and convection wavelength by allowing convective overturns to adjust to nonevolving plate geometries.

[4] Convective time dependence is promoted by an assortment of parameters including the presence of internal heating and system aspect ratio [e.g., *Travis et al.*, 1990a, 1990b; *Travis and Olson*, 1994; *Parmentier et al.*, 1994]. Stabilizing influences on convection planform include viscosity stratification [*Dubuffet et al.*, 2000] and steady plate motion [*Nettelfield and Lowman*, 2007]. Imposed, nonevolving plate motion has been shown to affect planform and convection wavelength in numerous studies [e.g., *Bunge and Richards*, 1996; *Ratcliff et al.*, 1997; *Zhong et al.*, 2000; *Monnereau and Quéré*, 2001; *Lowman et al.*, 2001; *Quéré and Forte*, 2006].

[5] Viscously stratified, vigorous, internally heated convection does not necessarily entail a highly time-dependent convective planform, even when a large degree of internal heating is present [*Dubuffet et al.*, 2000]. Plate boundary motion is required by the nature of plate tectonics rather than the behavior of convection. For example, asymmetric subduction results in plate boundary motion [*Zhong and Gurnis*, 1995] but because asymmetric subduction does not evolve naturally in a convecting fluid, a mechanism for driving the migration of downwellings may not be present in all convecting systems.

[6] Previous 2-D and 3-D convection studies featuring model plates and high Rayleigh number internally heated convection have concluded that the combination of plate motion and internal heating results in a behavior characterized by intermittent reorganizations of the convection planform and surface velocities, punctuating longer periods of relatively steady plate motion [*Lowman et al.*, 2001; *King et al.*, 2002; *Lowman et al.*, 2003; *Koglin et al.*, 2005]. However, these findings were obtained with the imposition of fixed plate geometries. Recent two-dimensional modeling allowing for plate boundary evolution found that intermittent mantle flow reversals disappeared once plate boundary motion was enabled [*Gait and Lowman*, 2007]. Indeed, it appears unlikely that the flow reversal mechanism exhibited by 180° changes in plate direction in two-dimensional studies has played a role in the history of the Earth. The time periods occurring between reversals scale to several hundred millions of years, a period long enough for an evolving system of plates to drastically change its configuration. However, the intermittent reorganization events observed in 3-D studies featuring plates do not require 180° changes in plate direction and occur much more frequently than flow reversals in two dimensional simulations [*King et al.*, 2002]. In a 3-D system able to reorganize itself through adopting a range of plate motions, the issue of whether plate boundary evolution occurs rapidly enough to eliminate reorganization events has yet to be addressed.

[7] Mantle convection wavelength and time dependence are affected by, among other things, both plate dimensions [*Gurnis and Zhong*, 1991; *Zhong and Gurnis*, 1993] and the viscosity stratification of the mantle [*Bunge et al.*, 1996, 1997]. We first examine a convective system featuring a lower mantle viscosity that is consistent with inferences based on long-wavelength geoid anomalies [e.g., *Hager*, 1984; *Richards and Hager*, 1984; *Ricard et al.*, 1984; *Forte and Peltier*, 1987; *King and Masters*, 1992] and independent constraints associated with observed long-term rates of polar wander [e.g., *Sabadini and Yuen*, 1989; *Spada et al.*, 1992]. Accordingly, we employ a reference viscosity profile featuring a lower mantle viscosity that increases by a factor of 30 from top to bottom. The profile is idealized and includes a rapid but smooth increase in lower mantle viscosity and a uniform viscosity upper mantle.

[8] More recent joint inversions of data associated with mantle convection and glacial isostatic adjustment suggest a wider range of lower mantle viscosity profiles are possible, including profiles allowing lower mantle regions that exceed upper mantle viscosity by up to a factor of $10^3$ [*Forte and Mitrovica*, 2001; *Mitrovica and Forte*, 2004]. Consequently, we extend our modeling to focus on assessing the role of depth-dependent viscosity on system time dependence when the lower mantle of our reference case is increased by factors of 3 and 10.

[9] The viscosity of the deep mantle is likely to play an important role in determining plate velocities. Evidence from self-consistent studies of mantle convection featuring complex rheologies tailored to produce plate-like surface motion suggest that in order to obtain sustained plate motion [*Richards et al.*, 2001; *Stein et al.*, 2004], a significant increase in mantle viscosity with depth may be required. By considering several mantle viscosity models in convection calculations featuring evolving plates, we are able to determine what effect viscosity depth dependence has on heat flow, plate velocity and boundary motion time dependence. We compare time dependence in systems featuring a simple condition for obtaining plate boundary evolution that is consistent with the calculated plate velocities and models that feature imposed static plate geometries. In total we present the findings from six calculations. All models feature dynamically determined evolving plate velocities.

## 2. Model Description

[10] We simulate convection in the Earth's mantle by modeling infinite Prandtl number thermal convection in an incompressible Boussinesq fluid with a Newtonian rheology. The nondimensionalized equations governing the evolution of the convection are derived from the conservation of mass, momentum and energy and take the form

$$\nabla \cdot \mathbf{v} = 0, \tag{1}$$

$$\nabla \cdot (\eta(z)\dot{\epsilon}) - \nabla P = -Ra_B T \hat{\mathbf{z}}, \tag{2}$$

and

$$\frac{\partial T}{\partial t} = \nabla^2 T - \mathbf{v} \cdot \nabla T + H, \tag{3}$$

respectively. The quantities in the equations above are: $\mathbf{v}$, velocity; $\eta(z)$, depth-dependent dynamic viscosity; $\dot{\epsilon}$, the

strain rate tensor; $P$, pressure; $T$, temperature; and $t$, time. $Ra_B$ is the Bénard-Rayleigh number [*Chandrasekhar*, 1961] and is given by

$$Ra_B = \frac{g\alpha\Delta T d^3}{\kappa\nu}, \quad (4)$$

where $g$ is gravitational acceleration; $\alpha$ is thermal expansivity; $\Delta T$, is the superadiabatic temperature difference between the top and bottom boundaries; $d$, is the depth of the convecting layer; $\kappa$, is thermal diffusivity and $\nu$, is kinematic viscosity. The rate of internal heat generation is $H$.

[11] Calculations are performed in 3-D solution domains with dimensions of $3 \times 3 \times 1$. (The computational grids have $325 \times 325 \times 129$ nodes.) The solution domain sidewalls are periodic, thus we model connected (i.e., wrap around) flow. We specify a free-slip basal boundary condition. The convecting layer is confined between isothermal horizontal boundaries in all calculations.

[12] The vigor of the dynamically driven flow is determined by the Rayleigh number and internal heating rates specified in the calculations. In this study, we specify a Bénard-Rayleigh number of $5 \times 10^7$, based on the upper mantle viscosity. We specify a uniform internal heating rate with $H = 15$. This heating rate is based on the assumption that the rate of internal heating in the mantle is $4.7 \times 10^{-12}$ W kg$^{-1}$, roughly the heating rate estimated for the bulk silicate Earth derived from a chondritic starting condition [*Stacey*, 1992]. With this internal heating rate the ratio of the basal to the surface heat flux obtained in our calculations is between 0.35 and 0.45.

[13] A hybrid spectral finite difference scheme for 3-D convection previously described by *Gable et al.* [1991] has been used to solve the system of equations (1)–(3). The version of the code (MC3D) used to carry out these calculations has been modified in order to perform calculations on a multiprocessor platform. MC3D has been benchmarked for a variety of problems that do not include plates and in those cases shows excellent agreement with the results obtained from other numerical methods [e.g., *Travis et al.*, 1991; *Busse et al.*, 1993].

[14] We model plate motion by using a force balance method. Thus, we specify a finite thickness highly viscous layer at the top of our models and prescribe dynamically evolving piecewise uniform surface velocities throughout distinct plate interior regions. The plates in our calculations are passive and neither drive nor resist the convective flow. Our plate modeling method has been shown to reproduce the same behavior obtained using rheological plate modeling methods that include characteristics like non-Newtonian viscosities and models with strong slabs and weak plate boundaries [e.g., *King et al.*, 1992; *Koglin et al.*, 2005]. We model dynamic plates by continually updating the plate velocities so that the integrated shear tractions on the base of each plate vanishes at all times [e.g., *Gable et al.*, 1991]. Thus plate velocities evolve to reflect the distribution of buoyancy within the plate and underlying fluid. The resulting condition is consistent with a rigid plate uniformly distributing the stresses applied at its base. The high-viscosity layer at the top of the models acts as a first-order approximation for the stiffness associated with the Earth's cold lithosphere.

[15] We focus on determining what effect evolving plate boundaries have on the time dependence of plate velocities and surface and basal heat flows. We investigate six convection models featuring different ratios of lower to upper mantle viscosity and compare three pairs of calculations, where each pair of calculations is started from the same initial conditions. The difference between the calculations comprising each pair is that in one case the plate boundaries remain fixed while in the other case, plates evolve. Plate velocities evolve dynamically in all cases in order to satisfy the constraint that the integrated shear stresses acting at the base of each plate sum to zero at all times.

[16] Each of the calculations examined features four plates and each plate has a simple polygonal morphology. Plate boundaries are straight lines. A model triple junction is formed wherever three plates meet. Each polygon line segment representing a section of a plate boundary joins two triple junctions. To model plates with evolving shapes, we migrate the model triple junctions. Line segments defining plate boundaries therefore move in order to continue to connect the same pair of triple junctions at all times. (In theory, a line segment defining a plate boundary can be severed if a triple junction migrates across it and when this occurs it can result in the division of one of the plates into two plates. Although our model is designed to allow for this occurrence, no such evolution develops in the calculations presented here.)

[17] As on the Earth, triple junctions are formed in our calculations at any point where three plates meet, however, their movement does not simulate the motion of real terrestrial triple junctions. The model triple junctions are moved with a velocity equal to the mean velocity of the three adjacent plates. The velocity of all triple junctions is determined in the same manner, regardless of the types of boundaries (e.g., convergent, divergent or transform) from which they form. Although this makes the evolution of the triple junctions in our model simplistic, in comparison to cases where the geometry is required to remain fixed, our model does allow us to compare how a convecting system featuring dynamically determined plate velocities may behave differently when the geometry of the plates is permitted to evolve. In addition, by using plate velocities to determine the rate of triple junction movement, the rate of evolution of the modeled plate system is able to dynamically respond to the time-dependent vigor of the convection.

[18] The plate velocities at the previous time step are used to move the model triple junctions (and therefore plate boundaries) prior to solving for flow. The flow solution obtained is a superposition of the buoyancy driven flow and the flow determined by the motion of each plate. To solve for the flow at one time step requires $2*(n + 1)$ solutions of the flow equations, where $n$ is the number of plates in the system. (In these calculations $n = 4$.)

[19] In order to model evolving plate shapes and sizes, we couple a finite element mesh generation code (The Los Alamos Grid Toolbox, LaGriT, Los Alamos National Laboratory, http://lagrit.lanl.gov, 2007) that takes MC3D's output of plate velocities to calculate triple junction motion. The finite element code represents the plates using a two-dimensional triangulation, migrates the model triple junctions on the basis of the plate velocities, and manages the mesh evolution and modification necessary to deform the

plates. LaGriT uses a collection of triangles to define each polygonal plate, these polygons are used to interpolate plate positions onto the surface of the high-resolution Cartesian grid describing the geometry of the four plates. This grid is used to compute the force balance on each plate. Grid nodes adjacent to plate boundaries are weighted to reflect the proportion of each plate associated with the node and the velocity boundary conditions in MC3D are adjusted accordingly at such locations.

[20] Below any linear plate boundary where the motion of the neighboring plates produces net convergence, our calculations result in the appearance of cold downwelling sheets. The cold sheets are fed by the motion of the model plates toward the plate boundary where cold material is forced downward. Because the plate velocities differ on each side of the boundary, and the plate boundaries are in motion, the downwelling does not receive an equal flux of material from each neighboring plate. However, the downwelling sheets in our calculations do not model true subducting slabs formed from just one plate at a convergent boundary. Similarly, the divergent plate boundaries in the calculations do not emulate symmetric seafloor spreading.

[21] We focus on examining the effect of viscosity stratification on the relative motion of plate boundaries and thermal features in the deep mantle. In particular, we examine the affect of lower mantle viscosity on the time dependence of heat flux and plate velocity. Consequently, we choose an idealized mantle viscosity profile. The calculations presented feature a nondimensional depth-dependent viscosity $\eta(z)$ characterized by an upper mantle viscosity of unity and an increase in lower mantle viscosity with depth that follows a logarithmic trend. The calculations we investigate feature lower mantle viscosities that are 30, 90 and 300 times more viscous than the upper mantle. The exact viscosities specified are

$$\eta(z) = 1000 \qquad 0.953d \le z \le d$$

$$\eta(z) = 1 \quad 0.769d \le z < 0.953d$$

$$\eta(z) = 1 + \frac{\eta_o^{-1}}{\log(100)} \log\left(1 + 99\left(\frac{0.769d - z}{0.769d}\right)\right) \qquad 0 \le z < 0.769d, \tag{5}$$

where $z$ is the height above the core-mantle boundary and $\eta_o$ = 30, 90 or 300. The viscosity of the plates is 1000 times greater than the mantle below and the plates have a thickness of $0.047d$.

[22] In order to obtain an initial thermal field for each of the three pairs of calculations investigated, we first obtain a two-dimensional ($x$, $z$) solution for convection with the specified viscosity and thermal parameters described above. The 2-D solution is obtained in an aspect ratio 3 model featuring a pair of equal size plates. The 2-D calculations are integrated forward in time until reaching a point where they exhibit neither long-term heating nor cooling trends. The two-dimensional solutions are then projected in the third ($y$) dimension to produce fields that occupy $3 \times 3 \times 1$ volumes. The 3-D fields are subsequently integrated forward in time with the static plate boundaries shown in Figure 1. The results presented here were obtained starting with an initial condition that was arbitrarily chosen at a time after the 3-D calculation reached a state where any clear heating or cooling has ceased.

[23] *Lowman et al.* [2001] previously examined two-dimensional aspect ratio 12 systems featuring plates with fixed boundaries but dynamically determined velocities calculated in an identical manner to those calculated here. These authors found that when the number of plates in a system is increased, the same number of convection cells still develop if the heating and viscosity characteristics remain unchanged. This is because there is no constraint in the modeling that would stop two or more plates from moving in tandem. Thus, the four plates specified in our initial condition are free to move like two plates if that is what the heating mode and viscosity structure demand.

[24] In the sections that follow we convert the nondimensional output of our calculations to dimensionalized times and velocities. To calculate the dimensional values we take the mantle depth, $d$, to be 2900 km and the diffusion time, $d^2/\kappa$, to be 270 Ga. This time implies that the thermal diffusivity of the mantle, $\kappa$, is $10^{-6}$ $m^2s^{-1}$. Given these dimensional scales for distance and time, dimensional velocities are obtained from nondimensional velocities by multiplying by $1.07 \times 10^{-3}$ cm/a.

## 3. Results

### 3.1. Plate Velocity

[25] Figure 1 shows four temperature field snapshots from a calculation featuring a lower mantle that is 30 times more viscous than the upper mantle. In order to reveal features in the system interior (below the cold upper thermal boundary layer) the top $0.047d$ (136 km) of the temperature fields have been omitted. The cooler (blue) isosurface corresponds to a temperature of 0.59 and the warmer (orange) isosurface corresponds to a temperature of 0.89. The globally averaged mean temperature of the system remains close to 0.74. The horizontal slice through the fields are shown at a depth of $0.93d$. To the right of each temperature field snapshot we show a map of the geometry of the plates with the instantaneous corresponding plate velocities indicated by black arrows. A plate numbering convention is introduced in Figure 1a and referred to in the text below. The length of the arrows indicates the magnitude of the plate velocity. Each plate moves with a spatially uniform but temporally varying dynamically determined velocity. The plate configuration features eight triple junctions within the periodic (wrap around) solution domain and is identical to the plate configuration employed in a previous study by *King et al.* [2002]. There are no triple junctions along the boundaries of the solution domain. The plate shapes and sizes remain fixed during the entire calculation. The coordinate origin of the sections is indicated at the lower left corner of Figure 1. In the remainder of this paper we refer to the calculation shown in Figure 1 as Model 30. (Note that in the remainder of this paper we present all temperature fields using the same color palette and consistently remove the top $0.047d$ (136 km) of the field while showing the temperature on a plane at a depth of $0.93d$.)

[26] The sequence depicted in Figure 1 illustrates temperature field evolution over approximately 40% of the total period examined by our calculation. The features depicted are typical of those characterizing the system during its

entire evolution. Cold downwelling sheets descend into the mantle below convergent plate boundaries and spread across the base of the system. Between the cold regions at the base of the system a network of sheet-like instabilities rise from the bottom thermal boundary. Where these weak upwelling sheets intersect, stronger columnar-type upwellings form and traverse the entire mantle depth.

[27] During the period depicted in Figure 1 plate velocities in Model 30 remain quite steady. For example, Plate 2 moves in a direction described by a vector rotated between $-35°$ and $-45°$ relative to the positive $x$ axis. Plate 4 moves similarly but in the opposite direction. During the entire period modeled, the motion of the plates supplies cold material to a dominant downwelling sheet that forms below the boundary between the plates. There are also gradual changes in plate velocity that result in the appearance and disappearance of two other convergent plate boundaries during the period modeled.

[28] In Figure 2 we show time series of the plate velocity magnitudes and the direction of the plate motion. Plate motion direction is indicated in all cases by plotting the angle made between the velocity vector of the plate and the positive $x$ axis.

[29] During the period examined, the motion of Plate 1 changes by approximately 90° and Plate 3 changes direction by 60°. The changes in direction occur gradually and result in the formation and disappearance of downwellings between Plate 1 and its neighbors. For example, while Plate 1 is moving almost parallel to the $y$ axis between 160 and 380 Ma a downwelling sheet appears between Plate 1 and Plate 3. Before and after this period the downwelling is not present. At the end of the sequence the plate motion and temperature field are very similar to the plate motion and temperature field at the start of the sequence. In general, the plate velocities in Model 30 fall in the range 0.8 to 2.7 cm/a. The mean surface velocity is approximately 1.6 cm/a when averaged over the 540 Ma period described.

[30] We now consider the effect of plate boundary evolution on the time dependence of the plate velocities and the evolution of the thermal fields in our model. Figure 3 shows four temperature field snapshots and corresponding plate geometries from Model 30e. Model 30 and Model 30e start with the same initial condition. The snapshots shown in Figure 3 are taken at approximately the same intervals as the snapshots shown in Figure 1.

[31] The plates evolve according to the criterion described in Section 2. The shapes of the plates change considerably but the surface area of each plate does not change dramatically. Plate velocities, indicated by the black arrows on the plate geometry maps, are more time dependent than in Model 30. As the plates evolve, the positions of the downwelling sheets shift dramatically so that by the end

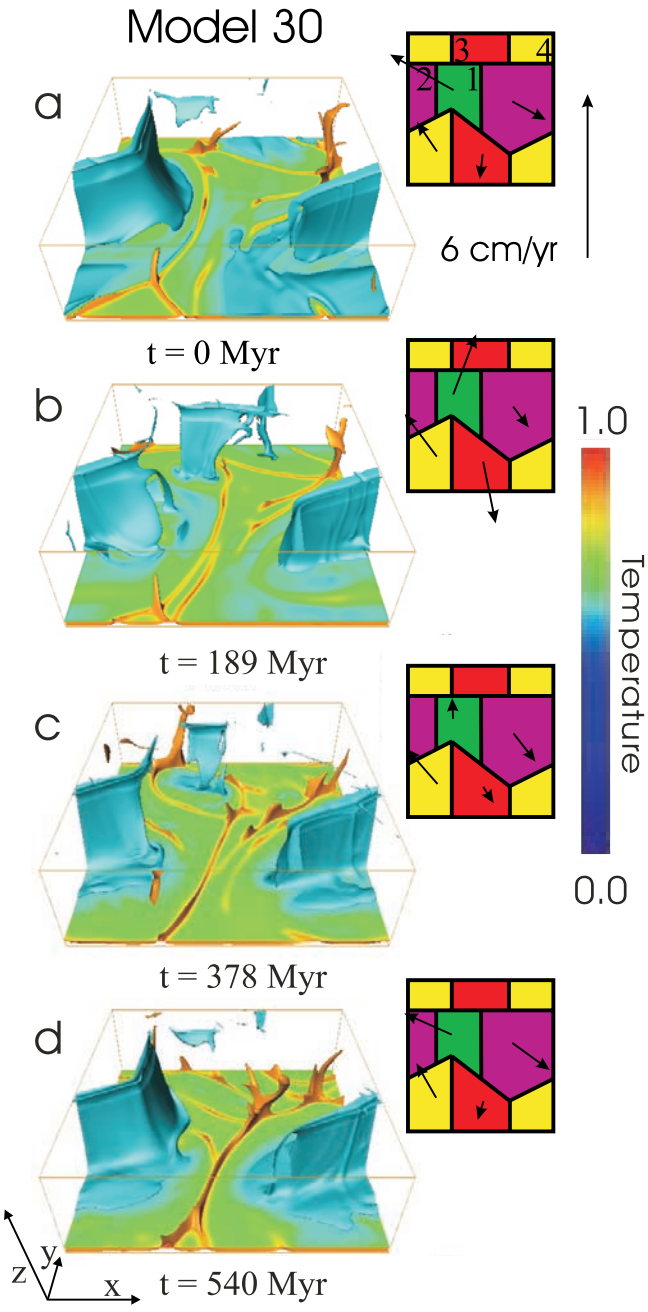


**Figure 1.** Normalized temperature field and plate geometry for Model 30. Temperatures are indicated using a linear scale where 1.0 corresponds to the temperature at the hot base of the calculation and 0.0 corresponds to the temperature at the cold surface. The hot (orange) isosurface corresponds to a temperature of 0.89 and the cooler (blue) isosurface corresponds to a temperature of 0.59. The top 4.7% of the fields have been removed, in order to allow observation of the fluid interior. The horizontal slice near the base of the system is at a depth of 0.93 times the total layer depth. The times quoted below each section give the dimensionalized time that has elapsed since the calculation's starting point and corresponds to the times indicated in Figure 2. The sections on the right are maps of the plate shapes and positions. Each of the plates (1–4) described in the text is labeled in Figure 1a and is indicated by a unique color throughout. Plate velocities at the times corresponding to the temperature field snapshots are indicated by black arrows. The arrow tails are placed at the center of the associated plate. The length of the arrows is scaled to the (6 cm/a) magnitude of the vertical plate velocity vector drawn above the temperature scale.

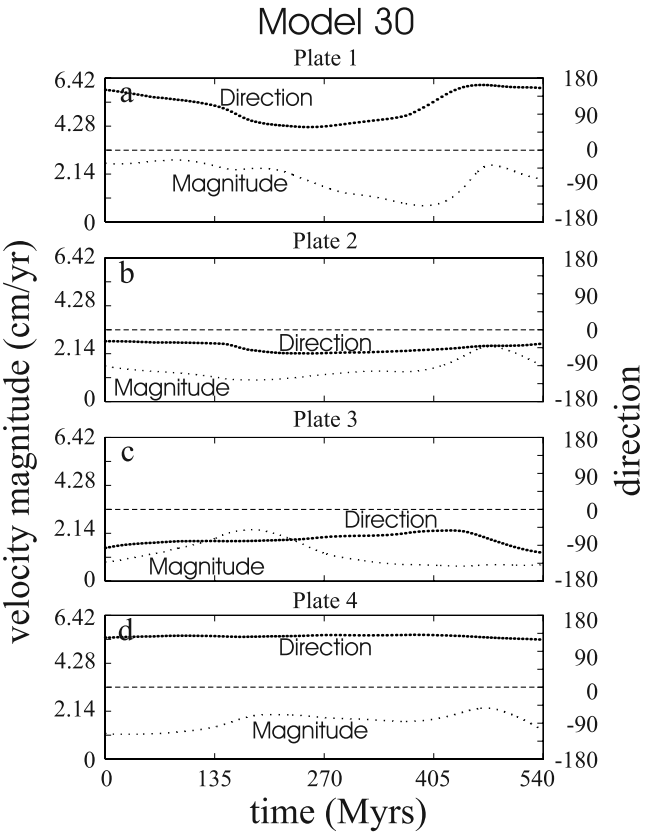


**Figure 2.** Plate velocity magnitude and direction time series from Model 30 for (a) plate 1 (green), (b) plate 2 (magenta), (c) plate 3 (red), and (d) plate 4 (yellow). The direction of the plate motion is given by measuring the angle between the plate velocity vector and the positive *x* axis (shown in Figure 1 and all subsequent temperature field figures). Angles measured counterclockwise in the *x*-*y* plane are positive.

of the period examined the temperature field bears little resemblance to the initial condition. However, overall the field is characterized at all times by the presence of downwelling sheets and upwelling columnar-type features.

[32] Figure 4 shows the time series of the plate velocity magnitudes and the plate directions in Model 30e using the same format as Figure 2. The plate velocities vary from 0.1 to 5.4 cm/a. In addition, changes in magnitude and direction occur more rapidly than in Model 30. For example, at time 200 Ma, Plate 1 begins a change in direction of approximately 100° over a period of 25 Ma. Similar changes in direction occur for other plates. Plate 4 abruptly changes direction at ~370 Ma; also changing direction by 90° in a period of ~25 Ma and eventually completing a change in direction of approximately 180°. We note that the changes in plate direction described are not necessarily accompanied by comparable, temporally coincident, changes in the directions of the other plates. A large change in direction of one plate can be compensated by a combination of changes in velocity magnitude, and small directional changes, in the other plates.

[33] We now consider a pair of models with a lower mantle that is 90 times more viscous than the upper mantle. Figure 5 shows an initial and final snapshot of the temperature field from Model 90. The snapshots are separated by an interval of 972 Ma. The average nondimensional temperature during the period modeled is 0.72 and the hot and cold isosurfaces shown in Figure 5 are 0.87 and 0.57, respectively. The plate boundaries in Model 90 remain fixed in identical positions to that specified in Model 30. The increase in lower mantle viscosity of a factor of three,

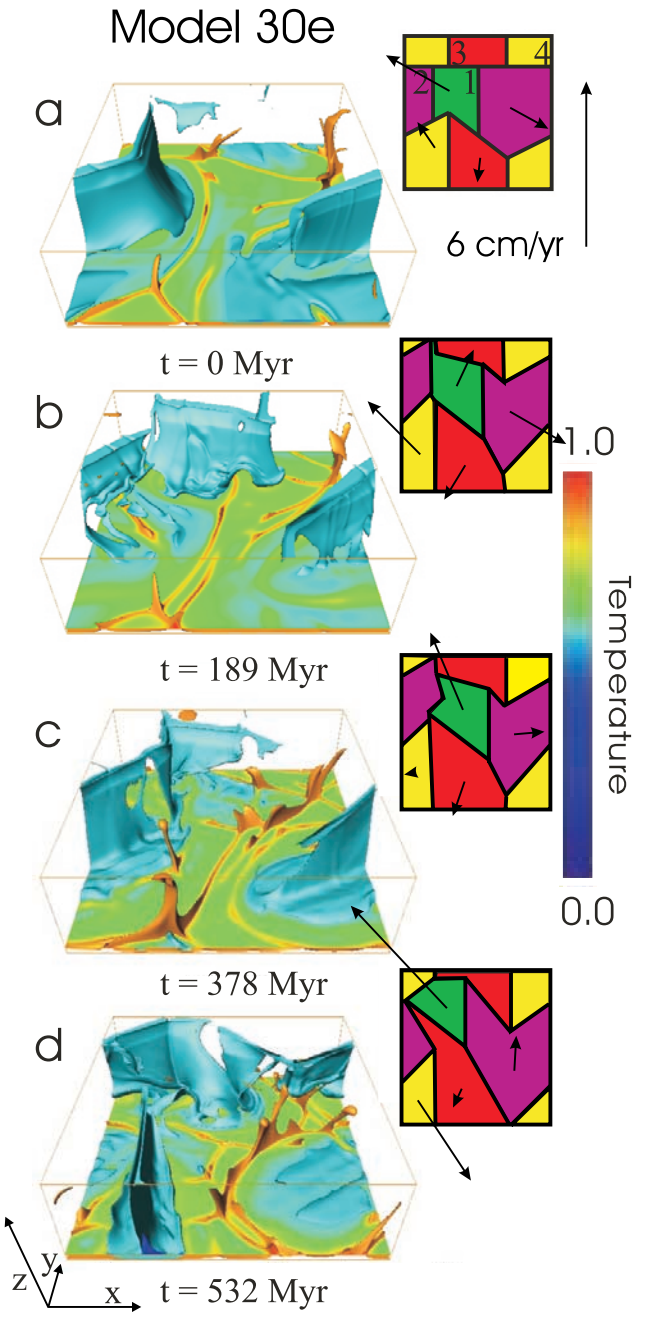


**Figure 3.** Normalized temperature fields and corresponding plate geometries for Model 30e. The temperature field isosurfaces and horizontal slice shown correspond to the same values and depth, respectively, as those in Figure 1. The arrows indicating the plate velocities shown in each section are drawn to the same scale as the arrows in Figure 1.

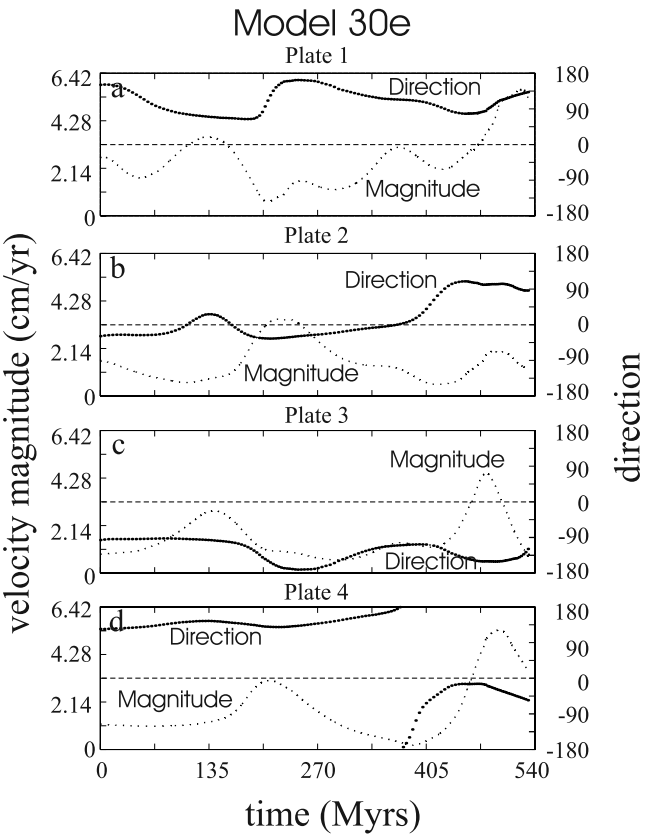


**Figure 4.** Plate velocity magnitude and direction time series from Model 30e for (a) plate 1 (green), (b) plate 2 (magenta), (c) plate 3 (red), and (d) plate 4 (yellow). Plate velocity direction is represented as in Figure 2.

compared with Model 30, results in a steadier flow. Although the convection in this model is time dependent the convective planform, including the position of the upwellings, remains constant during the entire period examined. The upwellings in this model are also more robust than the upwellings in Model 30. The upwellings in Model 90 are more plume-like and less mobile.

[34] Figure 6 shows the velocity time series data from Model 90. There are no substantial changes in plate direction during the period examined. Plate velocities rise and fall periodically and in unison. The average plate velocity is 1.34 cm/a, ~17% less than in Model 30.

[35] Figure 7 shows four snapshots from Model 90e depicting the temperature field and plate positions at intervals of 324 Ma. Model 90e starts with the same initial condition as Model 90 but features evolving plates governed by the conditions specified in Section 2. As in Model 90 the temperature field in Model 90e is dominated by cool downwelling sheets and columnar upwellings. In contrast to Model 30e, the plate shapes and sizes evolve dramatically in this calculation so that the plate areas and locations at the end of the sequence differ significantly from the initial plate areas and locations. For example, Plate 4 (yellow) shrinks to approximately one-quarter its initial area. The substantial rearrangement of the plates results in a repositioning of the downwelling features in the model that completely differs from the initial positions of the downwellings. However, the number of upwellings as well as their approximate locations change very little during the period examined.

[36] Figure 8 shows the velocity time series data from Model 90e. In contrast to the velocities from Model 90, the model with plate boundary evolution features rapid changes in the direction of plate motion and a wider variation in the magnitude of the plate velocities observed. For example, at 325 Ma, Plate 1 changes direction by rotating through roughly 180° in a period of approximately 25 Ma. This event is part of a major reorganization of the surface motion that includes a change in direction of Plate 3 by 135° and increases in the magnitudes of the velocities of Plates 2 and 4 by roughly a factor of 3. Interestingly, the directions in which Plates 2 and 4 are moving is not effected by the reorganization event at 325 Ma. A second, less dramatic,

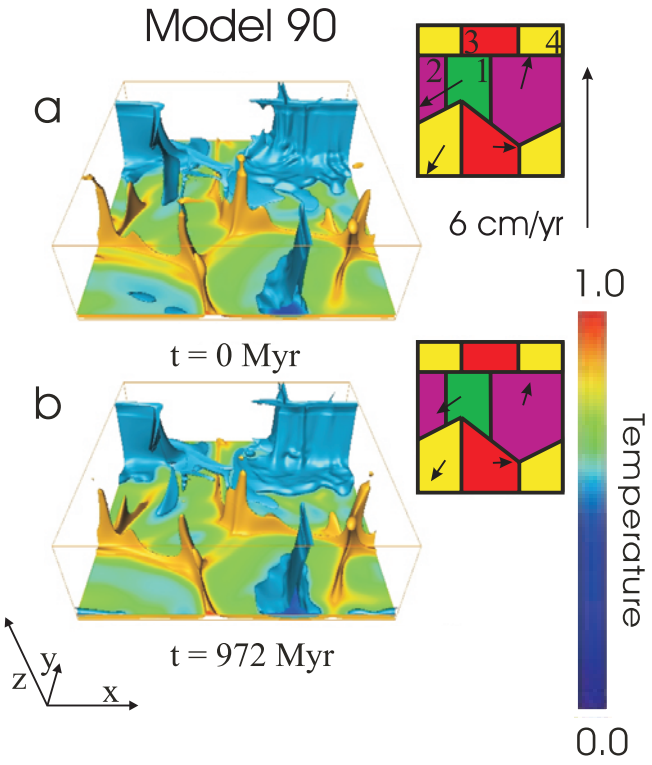


**Figure 5.** Normalized temperature fields and plate configuration for Model 90. The hot (orange) isosurface corresponds to a temperature of 0.87 and the cold (blue) isosurface corresponds to a temperature of 0.57. The top 4.7% of the fields have been removed, in order to allow observation of the fluid interior. The horizontal slice near the base of the system is at a depth of 0.93 times the total layer depth. The times quoted below each section give the dimensionalized time that has elapsed since the calculation's starting point and corresponds to the times indicated in Figure 6. The sections on the right are maps of the plate positions. Each of the plates (1–4) described in the text is labeled in Figure 5a and is indicated by a unique color throughout. Plate velocities at the times corresponding to the temperature field snapshots are indicated by black arrows. The arrows indicating the plate velocities shown in each section are drawn to the same scale as the arrows in Figures 1 and 3.

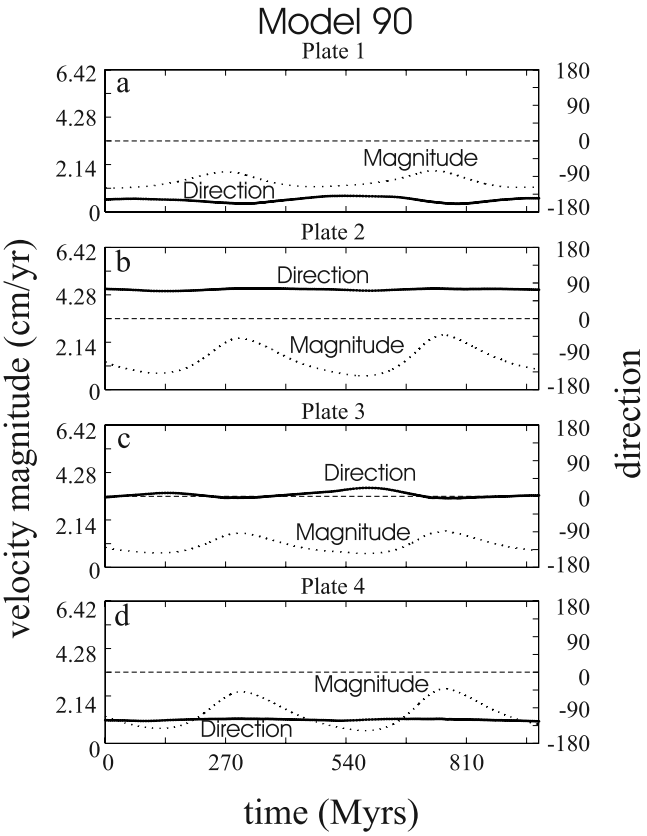


**Figure 6.** Plate velocity magnitude and direction time series from Model 90 for (a) plate 1 (green), (b) plate 2 (magenta), (c) plate 3 (red), and (d) plate 4 (yellow). Plate velocity direction is represented as in Figure 2.

reorganization event starts at 865 Ma. Plate motions are largely steady between the reorganization events despite the significant evolution of the plates between 325 and 865 Ma.

[37] The final pair of calculations we examine have a lower mantle viscosity that is 300 times greater than the upper mantle viscosity. Figure 9 shows initial and final snapshots from the calculation featuring nonevolving plate boundaries, Model 300. The mean temperature of Model 300 during the 1194 Ma time period examined is 0.68. The blue and yellow isosurfaces shown in Figure 9 have temperatures of 0.53 and 0.83, respectively. As in the previous models, the downwellings in Model 300 have a sheet-like morphology. The upwellings are sheet-like in the bottom half of the model but take on a columnar morphology as they reach the upper half of the system. As hot material reaches the constant viscosity upper mantle it rises more rapidly so that the upwellings narrow in the upper mantle. This phenomenon was present in the earlier calculations presented but is particularly evident in this model because of the magnitude of the viscosity contrast. During the period examined Model 300 displayed an extremely steady planform. The positions and the number of upwellings do not change nor do the position of the downwellings.

[38] Figure 10 shows the velocity time series data from Model 300. During the period shown, the mean spatially averaged velocity of the surface is 1.05 cm/a. Both the directions and magnitudes of the individual plate velocities are much steadier than in the previous models examined.

[39] Figure 11 shows four temperature field snapshots from Model 300e. This calculation starts from the same initial condition as Model 300 and is identical to that model with the exception that Model 300e allows for plate boundary evolution. The plate shapes and positions at the time of

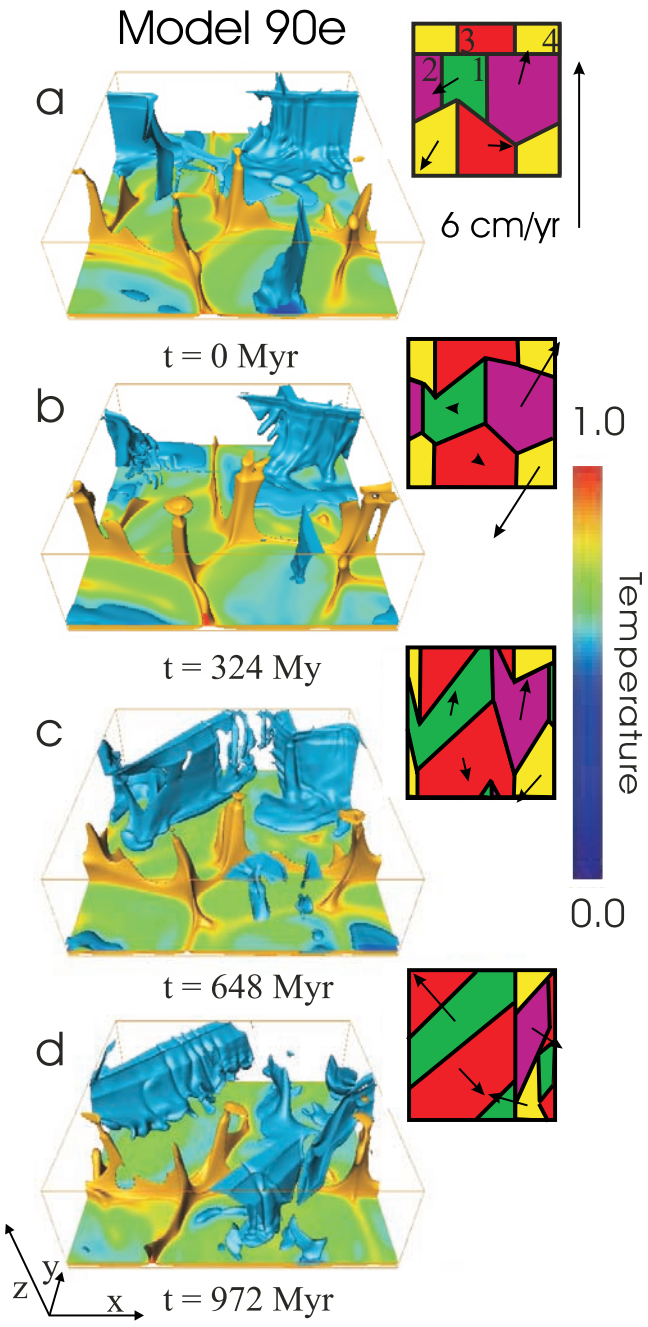


**Figure 7.** Normalized temperature fields and corresponding plate geometries for Model 90e. The isosurfaces and horizontal slice shown correspond to the same values and depth, respectively, as those in Figure 5. The arrows indicating the plate velocities shown in each section are drawn to the same scale as the arrows in Figures 1, 3, and 5.

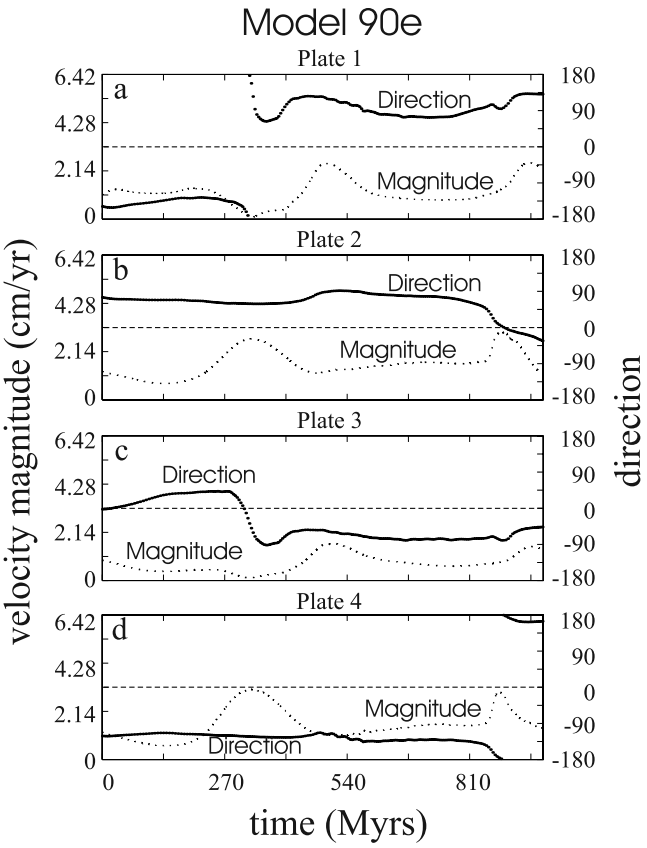


**Figure 8.** Plate velocity magnitude and direction time series from Model 90e for (a) plate 1 (green), (b) plate 2 (magenta), (c) plate 3 (red), and (d) plate 4 (yellow). Plate velocity direction is represented as in Figure 2.

each snapshot are shown with each corresponding temperature field. During the period modeled the plate shapes change dramatically so that the initial and final plate morphologies are completely different. Model 300e features an evolving network of downwelling sheets that shift steadily as the plates evolve. As a result, the positions of the downwellings in the final temperature field shown in Figure 11 are very different from the positions in the initial field. However, despite the evolution of the surface and the movement of the downwellings, the columnar upwellings in the model move very little. In addition, no new upwellings appear and no existing upwellings appear to weaken.

[40] Figure 12 shows the velocity time series data from Model 300e. The mean velocity of the plates is lower than in the previous calculations featuring plate evolution. In addition, the mean surface velocity does not show the fluctuations exhibited in the previous models. Despite the movement of the plate boundaries and the evolution of the downwellings in Model 300e, there are no abrupt changes in either plate velocity magnitude or direction. The plate direction vector of one plate rotates by over 100° during the period modeled, but the change occurs gradually and velocity magnitude is not significantly affected.

### 3.2. Heat Flux

[41] Both the average surface and basal heat flux of a convecting system featuring plates are affected by factors such as the mean magnitude of the surface velocity, the time dependence of the surface velocity, the proximity of active upwellings to divergent plate boundaries and the motion (and appearance of new) downwellings [e.g., *Lowman et al.*, 2001]. The latter factor can increase basal heat flux by depositing cold material over the warm thermal boundary layer at the base of the system, thus raising the basal temperature gradient so that the heat flow into the mantle increases. Clearly, each of the factors listed above varies by differing degrees in the calculations presented in the previous section. Here we consider the mean heat flux in each calculation and examine the effects of both the evolving boundaries and the lower mantle viscosity on the heat flux.

[42] Figure 13a compares the time series of the surface and basal heat fluxes from Models 30 and 30e. Fluctuations are not restricted to the case featuring evolving plates,

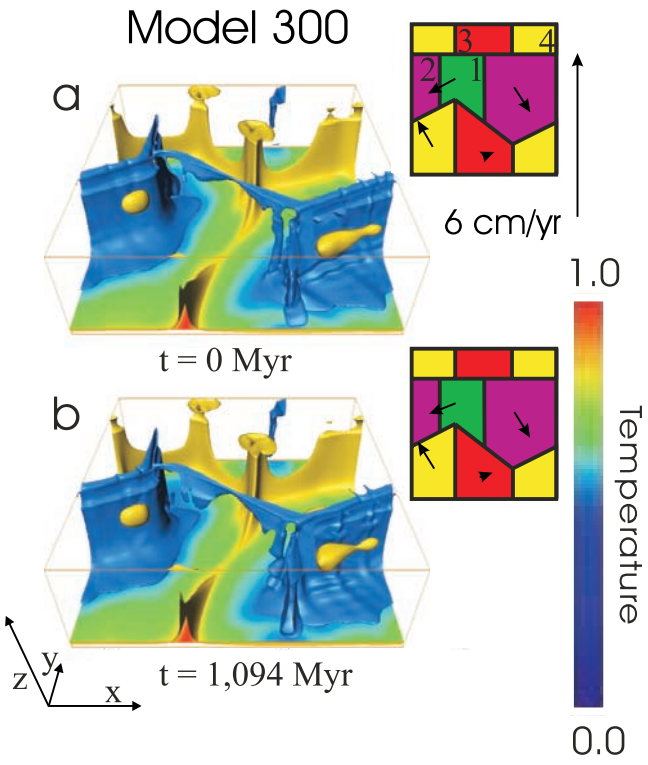


**Figure 9.** Normalized temperature fields and plate configurations for Model 300. The hot (orange) isosurface corresponds to a temperature of 0.83 and the cold (blue) isosurface corresponds to a temperature of 0.53. The top 4.7% of the fields have been removed, in order to allow observation of the fluid interior. The horizontal slice near the base of the system is at a depth of 0.93 times the total layer depth. The times quoted below each section give the dimensionalized time that has elapsed since the calculation's starting point and correspond to the times indicated in Figure 10. The sections on the right are maps of the plate positions. Each of the plates (1–4) described in the text is labeled in Figure 9a and is indicated by a unique color throughout. Plate velocities at the times corresponding to the temperature field snapshots are indicated by black arrows. The arrows indicating the plate velocities shown in each section are drawn to the same scale as the arrows in Figures 1, 3, 5, and 7.

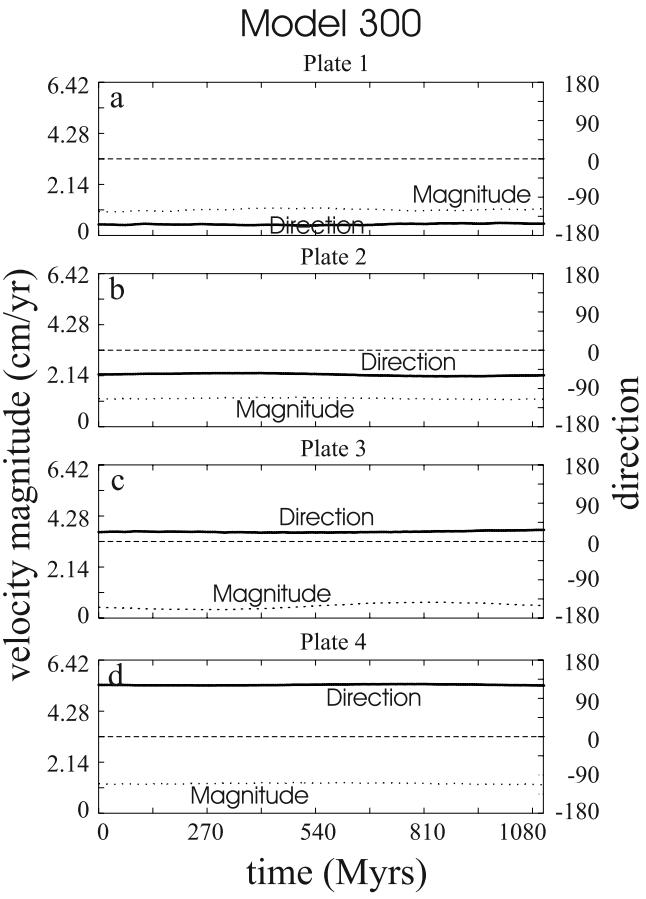


**Figure 10.** Plate velocity magnitude and direction time series from Model 300 for (a) plate 1 (green), (b) plate 2 (magenta), (c) plate 3 (red), and (d) plate 4 (yellow). Plate velocity direction is represented as in Figure 2.

however, during most of the period examined the basal and particularly the surface heat flux are both greater in that case. In addition, the plate reorganization events identified in the analysis of Figure 4 are manifested in the heat flux time series of Figure 13a by associated rises in the mean surface heat flux output. We find that surface heat flux may fluctuate by almost a factor of two in comparisons of minimum and maximum values. Basal heat flux varies by a smaller amount but clearly increases during the periods following increases in surface heat flux.

[43] Figure 13b shows the time series of the surface and basal heat fluxes from Models 90 and 90e from the periods examined in the previous section. The surface heat flux of the nonevolving model clearly exhibits a periodic variation correlating with the periodicity in the plate velocities. The surface heat flux of Model 90e is comparable in magnitude to the surface heat flux of Model 90 but does not exhibit the periodicity of the latter model. Model 90e features three periods of elevated surface heat flux during its evolution. These events peak at times 338, 513, and 945 Ma and correspond to the distinct increases in plate velocity magnitude shown in Figure 8. (Transient increases in velocity are experienced first by Plates 2 and 4, then by Plates 1 and 3 and finally by all four plates.) However, in contrast to the effect of the plate velocities on the surface heat flow, the basal heat flux in both Model 90 and Model 90e is very steady. It appears that the high-viscosity lower mantle might provide some buffering effect that reduces the effect of the arrival of cold material at the bottom boundary of the system, though the findings described here require a more systematic investigation of this phenomenon in order to confirm this suggestion.

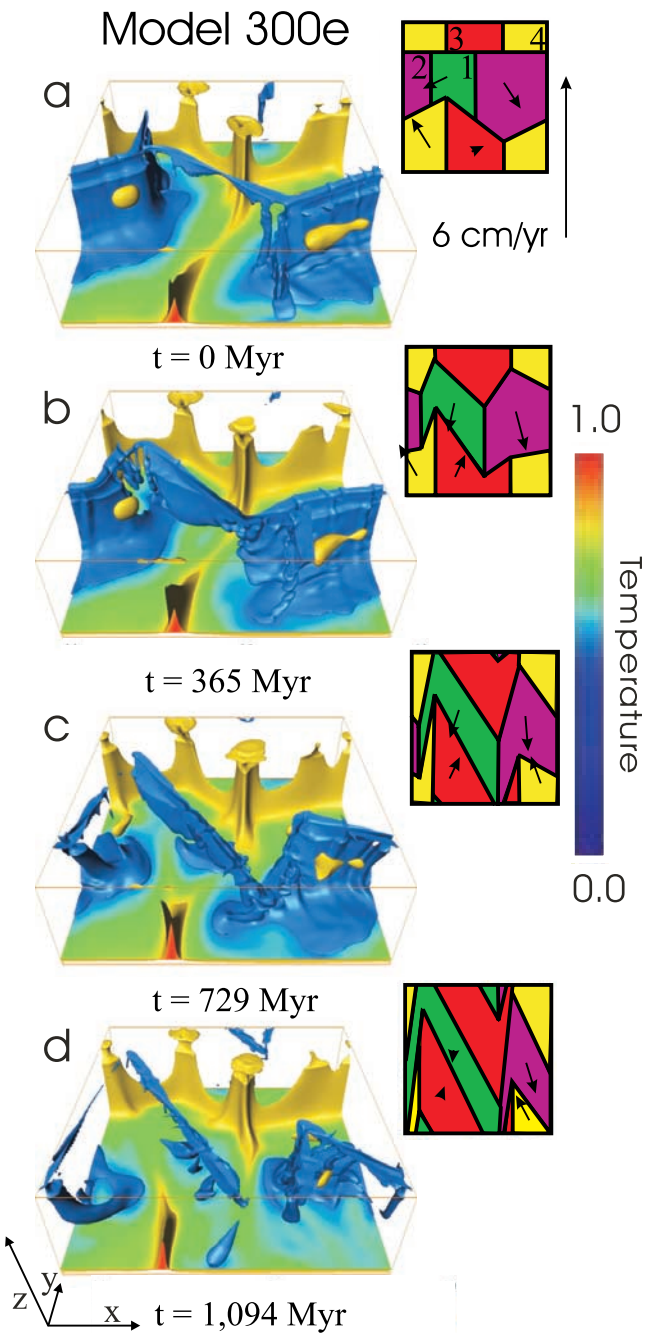


**Figure 11.** Normalized temperature fields and corresponding plate geometries for Model 300e. The isosurfaces and horizontal slice shown correspond to the same values and depth, respectively, as those in Figure 9. The arrows indicating the plate velocities shown in each section are drawn to the same scale as the arrows in Figures 1, 3, 5, 7, and 9.

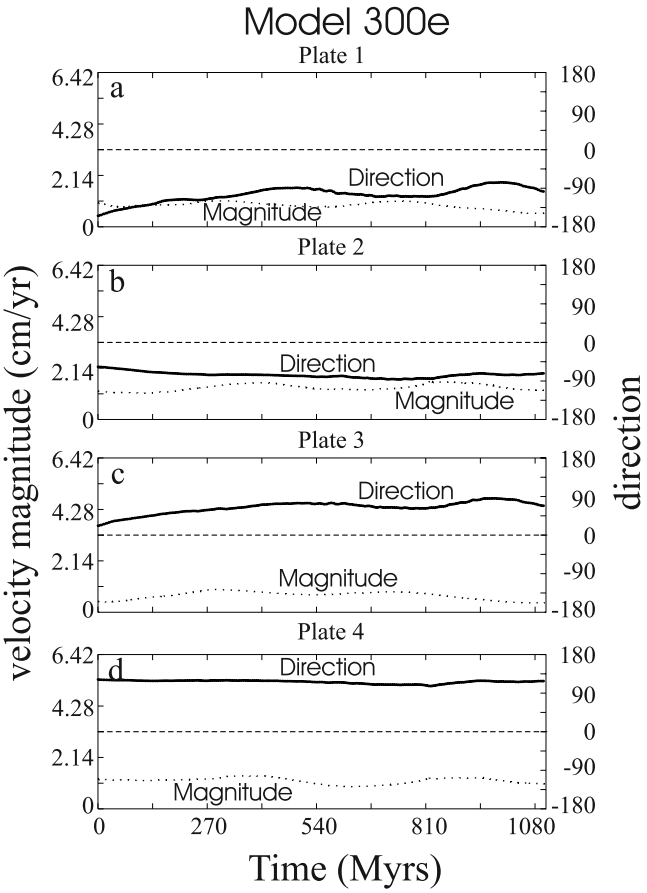


**Figure 12.** Plate velocity magnitude and direction time series from Model 300e for (a) plate 1 (green), (b) plate 2 (magenta), (c) plate 3 (red), and (d) plate 4 (yellow). Plate velocity direction is represented as in Figure 2.

[44] Figure 13c shows the surface and basal heat flux time series for Models 300 and 300e. Like the velocity time series, the heat flux time series for Model 300 vary less than in the lower-viscosity contrast models. The surface and basal heat fluxes from Model 300e exhibit only small fluctuations although both show a long period decreasing trend during the period examined. The minimal variation in surface heat flux in Model 300e is in contrast with Model 90e. In both models the plate boundary positions and the locations of the downwelling flow change dramatically. However, plate velocity magnitude varies more greatly in Model 90e.

[45] We note that in Models 90e and 300e in particular, the number and planform of the upwellings changes very little as the calculations evolve because they are anchored in the high-viscosity lower mantle. In contrast, movement of the downwellings is less inhibited since they originate in the lower-viscosity upper mantle. Thus the increased time dependence in the heat flux results from the motion of the plate boundaries rather than the appearance of new plumes.

## 4. Discussion

[46] The Rayleigh number specified in all of our calculations is based on the upper mantle viscosity, consequently, we quote the same Rayleigh number for all experiments. However, increasing the lower mantle viscosity changes the effective Rayleigh number of the system and therefore the magnitude of the plate velocities. Figure 14a shows time series of the mean surface velocity magnitude for each of the three models featuring nonevolving plate boundaries (note that because of the differences in plate size this is not the same as the mean plate speed). The time series shown for Models 30 and 90 exceed the periods considered in the previous section and illustrate the model behavior over longer periods. The decrease in the mean plate velocity as a function of lower mantle viscosity is clearly illustrated, as is the trend from erratic time dependence (Model 30), to a quasi-periodic time dependence (Model 90) and finally a relatively steady solution (Model 300).

[47] We specify a Rayleigh number that is slightly low for the Earth in order to obtain a numerically manageable problem (i.e., a problem that can be solved with the highest grid resolution possible in a reasonable amount of computer time). The magnitudes of the plate velocities obtained confirm that the effective Rayleigh numbers specified in this study are lower than the effective Rayleigh number of

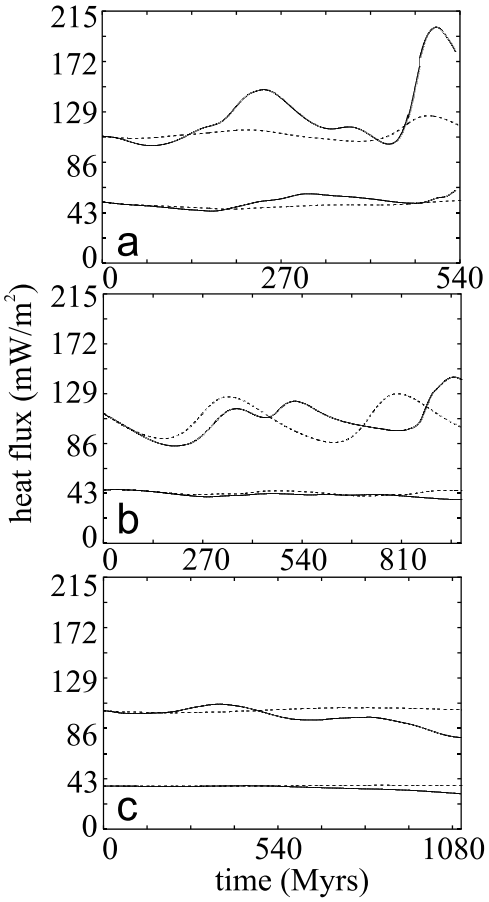


**Figure 13.** Surface and basal heat flux for (a) Models 30 and 30e, (b) Models 90 and 90e, and (c) Models 300 and 300e. Dashed curves correspond to cases with fixed plate boundaries. Solid curves correspond to cases with evolving plate boundaries. The curves showing starting values above 86 mW/m$^2$ correspond to the surface flux in all three cases.

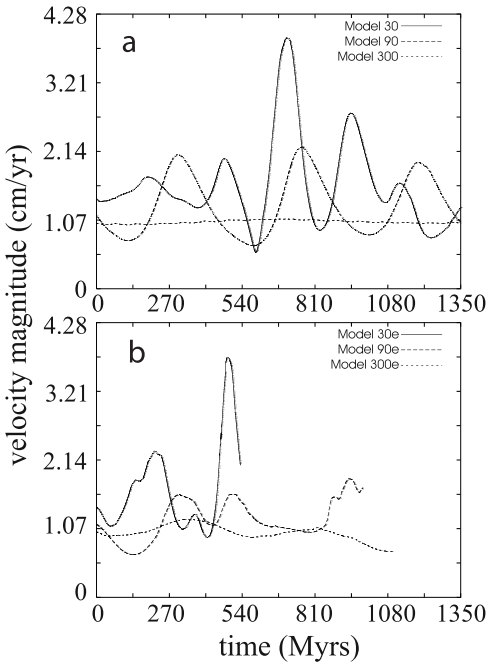


**Figure 14.** Mean surface velocity magnitude as a function of time. (a) The results for calculations with nonevolving plate boundaries, and (b) the results for calculations featuring evolving plate boundaries.

the Earth's mantle (*King et al.* [2002] previously suggested that a Rayleigh number of $5 \times 10^7$, based on an upper mantle viscosity, may be a factor of 3 to 4 times too low for modeling convection in the Earth's mantle if the lower mantle viscosity is a factor of 36 times greater than the upper mantle viscosity). In accord with lower plate velocities, we find that the mean upper thermal boundary layer thickness in Model 30 is about 40% thicker than the 100 km thick boundary layer typically quoted as representative of the Earth's plates. In a free-slip surface, isoviscous, bottom heated, convecting system, thermal boundary layer thickness decreases (approximately) in proportion to $Ra^{1/3}$ and surface velocities increase as $Ra^{2/3}$. This implies that the thermal boundary layer will increase in thickness by approximately 40% and the surface velocities will decrease by approximately a factor of 2 if a Rayleigh number is reduced by a factor of three. Internal heating and depth-dependent viscosity add complexity not accounted for in these scaling arguments, however, it appears that with the thermal boundary layer thicknesses we observe and dimensional velocities of almost 2 cm/a, our Model 30 calculation features an effective Rayleigh number 3 to 4 times too low for the Earth's mantle.

[48] The lower mantle in Model 90 is only 3 times more viscous than the lower mantle in Model 30 and a large difference in the convective vigor in these systems is not expected. We find the velocities in Model 30 a little higher than the velocities in Model 90. An order of magnitude change in Rayleigh number should correspond to a change in magnitude of surface velocities of roughly 4.6 if we assume the scaling for isoviscous, bottom heated convection is applicable. However, the average plate velocity in Model 300 is only about half of the average velocity found in Model 30 (this result suggests a Rayleigh number change closer to a factor of 3 which may be explained by the fact that effective Rayleigh number difference is not a true factor of 10 because of the unchanged upper mantle viscosities). Indeed, we found that the average surface heat flux in Model 30 was approximately 25% greater than in Model 300, indicating an increase in effective Rayleigh number of only 2, if we assume a $Ra^{1/3}$ scaling for the Nusselt number. Considering the changes in mean surface velocity and heat flux exhibited in this suite of models we suggest that although we change the lower mantle viscosity in our calculations by a factor of 10, the actual range of effective Rayleigh numbers considered is much less, probably about a factor of 3. The three models considered therefore appear to have effective Rayleigh numbers a factor of 3 to 9 times too low for the Earth.

[49] The evolving plate experiments presented in this study were integrated forward for differing time periods. However, the number of integration steps required to obtain these solutions is quite similar because of the effect of the lower mantle viscosity on the vigor of the convection. Thus, each solution required similar computational resources. Because of the computational effort required to integrate the solutions with evolving boundaries our observations are limited in time by practical considerations. In order to compare the variability in the behavior of these models and the period modeled relative to the vigor of the flow, it is instructive to consider a measure of the recycling of surface material.

[50] In Figure 14b we show the mean surface velocity magnitude time series from the three models featuring evolving plate boundaries. We note that the mean surface velocities for Model 30e, 90e and 300e are approximately 1.85 cm/a, 1.25 cm/a, and 1.01 cm/a, respectively. Thus, during corresponding periods of 540, 972, and 1094 Ma, a particle moving with a speed close to the mean surface velocity magnitude in these three models would travel between 10,000 and 12,000 km in the three cases (i.e., a distance in excess of the width of the solution domain). On the basis of these findings, we argue that the calculations corresponding to the time series in Figure 14b have each evolved for a period that should have allowed the plate shapes and sizes to change by similar amounts. Thus although the surface of Model 30e has not evolved as far from its initial state as the plate geometry in Models 90e and 300e (e.g., all the plates in Model 30e remain close to their original size), this is not because Model 30e has not be given as much time to evolve. In terms of surface transit times, each model has been allowed to evolve for a significant amount of time. Examining the magnitudes of the horizontally averaged mean horizontal velocities of our initial conditions indicates that the ratios of the mean basal velocities to the mean surface velocities is similar for all three viscosity cases. On the basis of this observation we suggest that the relative overturn times of the systems can be obtained by the ratios of the mean plate velocities. We note that vertical profiles of the horizontally averaged horizontal velocity indicate that some layering of the system has developed in Models 300 and 300e. For example, we find a confined sharp increase in the mean horizontal velocity just above the lower mantle (at a depth of $0.2d$).

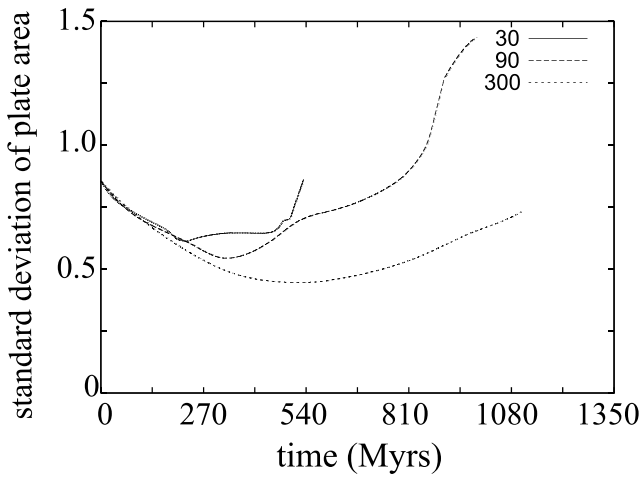


**Figure 15.** Time series of standard deviations of plates sizes for Models 30e, 90e, and 300e. Plate areas are normalized so that an area equal to the square of the system depth corresponds to a value of 1.0.

However, the lower mantle velocities in Model 300 show that overall the system convects as a single layer and that the highest lower mantle velocities exist at the base of the system as in Models 30 and 90.

[51] Figure 14b shows that the introduction of evolving boundaries eliminates periodic as well as steady behavior. However, velocity fluctuations decrease in magnitude as the lower mantle viscosity is increased. Maximum mean surface velocity magnitude can exceed the minimum mean surface velocity magnitude by a factor of 4 in Model 30 because of the effect of a plate reorganization event. Rapid changes in plate direction are also responsible for rises in mean plate velocity and average surface heat flux in Model 90e, although the maximum increase in average velocity is a factor of 2.5 and the three distinct periods of high velocity observed in Model 90e are less dramatic increases than in Model 30e. Model 300e does not feature any flow reorganization events nor rapid increases or decreases in average surface speed but has a mean surface velocity that is clearly time dependent.

[52] In order to assess how quickly the plate boundaries in each model evolve and whether their evolutionary behavior differs, we have calculated time series of the standard deviation of the plate area in Models 30e, 90e and 300e. A large standard deviation implies that the calculation features a mixture of small and large plates. Figure 15 shows that initially the standard deviation of the plate areas in Models 30e, 90e and 300e evolves very similarly but that eventually the plate sizes start to evolve differently and at different rates. Plate areas cannot change as rapidly as plate velocities or heat flux, however, changes in the gradients of the time series of the standard deviations do appear in response to changes in plate velocities. Figure 15 shows that plate sizes evolve very smoothly during the entire evolution of Model 300e while periods of rapid evolution occur in Model 30e and 90e starting at times 485 and 865 Ma, respectively. Thus, although it allows significant surface evolution over long periods, we find a high-viscosity lower mantle appears to inhibit periods of rapid evolution.

[53] In a calculation featuring the same configuration of plates as our nonevolving models, *King et al.* [2002] observed 12 reorganization events in a nondimensional time period of 0.01125. This time corresponds to a little over 3 Ga using the dimensionalization factor applied in this paper. However, this dimensionalization does not account for the slightly low Rayleigh number values used in the calculation (comparable to the Rayleigh number used in our Model 30e). *King et al.* [2002] argued that plate velocities observed for the Earth can be used to infer a dimensional time scale for a calculation featuring a lower Rayleigh number than the mantle's. For example, a calculation in which a particle moving with the mean surface velocity has traveled a distance of $3.45d$ (10,000 km) has simulated $\sim$250 Ma of evolution if we assume the mean plate velocity is approximately 4 cm/a (a reasonable estimate of mean plate velocity). In order to compare our findings with the times quoted in the study by *King et al.* [2002] the times given in our discussion of Model 30e should be reduced by a factor of 250/540 Ma = 0.463. Accordingly, we would find that the pair of flow reorganization events exhibited in Model 30e are separated by approximately 80 Ma. Using the same adjustment of the time scalings, the 25 Ma periods quoted for the duration of the reorganization events in Model 30e would reduce to 11.5 Ma. This period is substantially greater than the reorganization periods of less than 3.75 Ma reported by *King et al.* [2002], however, the events in Model 30e are both examples of changes in direction of a minimum of 90°. We suggest that changes in direction by smaller angles will occur in less time. Small but rapid changes in direction are not observed in the calculations presented here.

[54] Rapid reorganization events interrupted periods of relatively uniform plate motion during the Cenozoic and Mesozoic [e.g., *Rona and Richardson*, 1978; *Gordon and Jurdy*, 1986; *Clague and Dalrymple*, 1987; *Stock and Molnar*, 1987; *Lithgow-Bertelloni and Richards*, 1995]. Our findings show that intermittent plate reorganization events arise naturally in an internally heated convecting mantle featuring plate-like surface motion and plate boundary evolution. These events occur without the prompting of continental collisions or other forcing of a tectonic origin. The behavior described is an inherent feature of the plate-mantle system we have modeled. Previous studies, limited to calculations with fixed plate geometries, showed that internal heating rate plays a critical role in determining the frequency of flow reorganization events in a convecting system with plates [*Lowman et al.*, 2003]. However, our study shows that flow reorganization behavior can be suppressed by an increase in lower mantle viscosity. If indeed the lower mantle's viscosity is hundreds of times greater than the upper mantle viscosity [*Forte and Mitrovica*, 2001; *Mitrovica and Forte*, 2004], our results indicate that it is unlikely that plate reorganization events could have been driven by thermal forcing in the mantle. Conversely, a lower mantle viscosity that is less than 100 times more viscous than the upper mantle average suggests that mantle driven plate reorganization could have occurred in the Earth's history.

[55] None of the major plates on the Earth shares more than one distinct unbroken boundary with any other plate.

Thus an important limitation of our study which may effect the time dependence of the solutions and direct applicability to the evolution of the Earth is the relatively small solution domain. In order to model plates that are different in size but with dimensions that are at least comparable in scale to the mantle depth, we specify only four plates. With a small number of plates and a wrap around boundary condition, each plate is forced into contact with the same neighbor along more than one boundary. Consequently, when one plate changes direction, its neighbor is affected by a plate changing direction along two of its boundaries. The development of a convergent boundary along one edge must therefore be accompanied by the development of a divergent boundary along the opposite edge. A system with a small number of plates must also feature a high degree of coupling between all of its plates. For example, a change in direction or speed of one plate is expected to cause a significant change in the velocity of a neighbor in order to satisfy the condition that net horizontal flow in the system vanish. In a system featuring twice as many plates it might be possible for one plate to change velocity while the other plates in the system individually change velocity by a relatively small amount. Calculations in larger solution domains featuring more plates may therefore exhibit some forms of behavior not displayed in the models presented here, in particular the large changes in direction that occur during the reorganization events described here may be less dramatic. However, we suggest the differences in time-dependent behavior resulting from the effects of upper mantle-lower mantle viscosity contrast and plate boundary evolution will follow the trends observed in this study.

[56] Our calculations neglect explicitly specifying a temperature-dependent viscosity as well as the presence of continental lithosphere. However, by specifying high-viscosity plates with a thickness comparable to the upper thermal boundary layer thickness, we simulate the effects of a temperature-dependent rheology in the lithosphere. In addition, previous benchmarking has shown that our plate modeling method reproduces the time-dependent behavior and velocities found in models featuring rheologically weak plate boundaries with strong lithospheres and slabs [e.g., *King et al.*, 1992; *Koglin et al.*, 2005]. We expect that specifying a temperature-dependent viscosity would have an effect on the mobility of features in the deep mantle in our calculations but do not expect lateral viscosity variations in the upper mantle to significantly affect the calculated plate velocities. The presence of lithospheric heterogeneities such as continents could profoundly affect the motion and evolution of the plates and should be the focus of future research on the time dependence of plate motion and heat flux.

[57] We implement a highly simplified method for emulating triple junction movement and plate boundary migration. However, we argue that because the rate at which plates evolve is governed by the dynamics of the system, our experiments model the feedback between mantle convection and the rate at which plate boundaries and velocities change. Our findings suggest that plate boundary evolution results in more variable, less predictable, surface velocity and spatially averaged heat flux, but that the presence of a high-viscosity lower mantle acts to reduce this variability. Future studies should investigate whether larger systems (Cartesian or full spherical shell models) exhibit similar time-dependent behavior.

## 5. Conclusions

[58] Model plates were included in three-dimensional mantle convection calculations capable of allowing for plate boundary migration. Time-dependent boundary motion was determined by the evolving velocities of the finite thickness rigid plates. The feedback between plate evolution and plate velocity was studied by comparing results from calculations featuring static and mobile boundaries. Three different viscosity contrast models were considered in examining the effect of plate boundary evolution on the time dependence of mantle heat flow and plate velocities.

[59] Plate velocity time dependence decreases with viscosity stratification. The difference between the mean surface velocities during periods of relatively fast and slow motion decreases as the viscosity contrast is increased. The combination of nonevolving plate boundaries and a factor of 300 increase in lower mantle viscosity results in nearly steady mean plate velocity. Allowing the plate boundary to evolve allows for gradual changes in the surface velocity. In comparison, the mean plate velocity in calculations featuring a factor of 30 increase in lower mantle viscosity exhibits fluctuations of a factor of more than four (Figure 14), regardless of whether plate boundary evolution occurs.

[60] The variations in mean plate velocity observed in our calculations with either a factor 30 or a factor of 90 increase in lower mantle viscosity (relative to the upper mantle viscosity) appear to be partly explained by the appearance of flow reorganization events in these models [e.g., *King et al.,* 2002]. Models 30, 30e and 90e each feature periods in which the motion of one or more plates rapidly and significantly changes direction. Model 90 does not exhibit this behavior during the period studied, suggesting that a combination of plate boundary evolution and a lower contrast in upper mantle and lower mantle viscosity give rise to the greatest degree of time dependence. In addition, variations in mean plate velocity magnitude are less dramatic in Model 90e than Model 30 or 30e, also suggesting that a higher contrast in upper and lower mantle viscosity dampens the system time dependence.

[61] The presence of plate reorganization events in calculations featuring evolving plate boundaries contrasts with the results found in 2-D studies of mantle convection featuring evolving plates [*Gait and Lowman*, 2007]. However, flow reorganization events in 2-D models necessarily entail 180° changes in plate velocity direction. Reorganization events in 3-D calculations may result in velocity direction changes of less than 90°. The conditions required to trigger flow reorganization in 3-D are therefore less stringent. As a consequence, flow reorganization can occur with a geophysically significant frequency in a 3-D setting.

[62] Our findings also indicate that surface heat flow is sensitive to mantle viscosity stratification and the evolution of plates. We find that surface heat flux can increase by approximately 100% following flow reorganization events. However, such large variations were only observed in Model 30e. Variations in surface heat flux in Model 90 and Model 90e are very similar despite the fact that the mean surface velocity in Model 90e does not vary as much as it does in the

static plate boundary case, Model 90. Basal heat flux variations are mild in amplitude and temporal gradient in all of our models. The greatest variability is in Model 30e where basal heat flux varies by up to 10% of the mean value.

[63] The findings presented here show that it is unlikely that plate reorganization events [*King et al.*, 2002] are driven by the movement of buoyant pockets in the mantle if lower mantle viscosity is a factor of 300 (or more) times greater than upper mantle viscosity. If mantle viscosity increases by this order then tectonic events appear to be the best candidate to explain inferred dramatic changes in plate direction (although a clear connection between tectonics and plate reorganization has not been demonstrated [e.g., *Richards and Lithgow-Bertelloni*, 1996]). However, flow reorganization events appear to be a common feature in a convecting system featuring plate evolution and vigorous convection (comparable to terrestrial mantle convection) when the ratio of lower mantle to upper mantle viscosity is less than a factor of 100. Given a mantle viscosity profile fitting this description, we suggest that plate reorganization driven by deeply placed buoyancy sources may have occurred in Earth's history.

[64] **Acknowledgments.** A.D.G. thanks NERC for financial support. J.P.L. is grateful to the NSERC of Canada for continued funding in planetary mantle dynamics (327084-06).

## References

Bercovici, D. (2003), The generation of plate tectonics from mantle convection, *Earth Planet. Sci. Lett.*, *205*, 107–121.

Bunge, H.-P., and M. A. Richards (1996), The origin of large scale structure in mantle convection: Effects of plate motions and viscosity stratification, *Geophys. Res. Lett.*, *23*, 2987–2990.

Bunge, H.-P., M. A. Richards, and J. R. Baumgardner (1996), Effect of depth-dependent viscosity on the planform of mantle convection, *Nature*, *379*, 436–438.

Bunge, H.-P., M. A. Richards, and J. R. Baumgardner (1997), A sensitivity study of three-dimensional spherical mantle convection at $10^8$ Rayleigh number: Effects of depth-dependent viscosity, heating mode, and an endothermic phase change, *J. Geophys. Res.*, *102*, 11,991–12,007.

Busse, F. H., et al. (1993), 3D convection at infinite Prandtl number in Cartesian geometry—A benchmark comparison, *Geophys. Astro. Phys. Fluid Dyn.*, *75*, 39–59.

Chandrasekhar, S. (1961), *Hydrodynamic and Hydromagnetic Stability*, Oxford Univ. Press, New York.

Clague, D. A., and G. B. Dalrymple (1987), The Hawaiian-Emperor volcanic chain, Part I. Geological evolution, *U. S. Geol. Surv. Prof. Pap.*, *1350*, 5–54.

DeMets, C., R. G. Gordon, D. F. Argus, and S. Stein (1990), Current plate motions, *Geophys. J. Int.*, *101*, 425–478.

DeMets, C., R. G. Gordon, D. F. Argus, and S. Stein (1994), Effect of recent revisions to the geomagnetic reversal time scale on estimates of current plate motions, *Geophys. Res. Lett.*, *21*, 2191–2194.

Dubuffet, F., M. Rabinowicz, and M. Monnereau (2000), Multiple scales of mantle convection, *Earth Planet. Sci. Lett.*, *178*, 351–366.

Forte, A. M., and J. X. Mitrovica (2001), Deep-mantle high-viscosity flow and thermochemical structure inferred from seismic and geodynamic data, *Nature*, *410*, 1049–1056.

Forte, A. M., and W. R. Peltier (1987), Plate tectonics and aspherical Earth structure: The importance of surface plates poloidal-toroidal coupling, *J. Geophys. Res.*, *92*, 3645–3679.

Gable, C. W., R. J. O'Connell, and B. J. Travis (1991), Convection in three dimensions with surface plates: Generation of toroidal flow, *J. Geophys. Res.*, *96*, 8391–8405.

Gait, A. D., and J. P. Lowman (2007), Time-dependence in mantle convection models featuring dynamically evolving plates, *Geophys. J. Int.*, *171*, 463–477, doi.1111/j.1365-246X.

Gordon, R. G., and D. M. Jurdy (1986), Cenozoic global plate motions, *J. Geophys. Res.*, *91*, 12,389–12,406.

Gordon, R. G., A. Cox, and C. E. Harter (1978), Absolute motion of an individual plate estimated from its ridge and trench boundaries, *Nature*, *274*, 752–755.

Gurnis, M., and S. Zhong (1991), Generation of long wavelength heterogeneity in the mantle by the dynamic interaction between plates and convection, *Geophys. Res. Lett.*, *18*, 581–584.

Hager, B. H. (1984), Subducted slabs and the geoid: Constraints on mantle rheology and flow, *J. Geophys. Res.*, *89*, 6003–6016.

King, S. D., and T. G. Masters (1992), An inversion for the radial viscosity structure using seismic tomography, *Geophys. Res. Lett.*, *19*, 1551–1554.

King, S. D., C. W. Gable, and S. A. Weinstein (1992), Models of convection-driven tectonic plates: A comparison of methods and results, *Geophys. J. Int.*, *109*, 481–487.

King, S. D., J. P. Lowman, and C. W. Gable (2002), Episodic tectonic plate reorganizations driven by mantle convection, *Earth Planet. Sci. Lett.*, *203*, 83–91.

Koglin, D. E., Jr., S. R. Ghias, S. D. King, G. T. Jarvis, and J. P. Lowman (2005), Mantle convection with reversing mobile plates: A benchmark study, *Geochem. Geophys. Geosyst.*, *6*, Q09003, doi:10.1029/2005GC000924.

Lithgow-Bertelloni, C., and M. A. Richards (1995), Cenozoic plate driving forces, *Geophys. Res. Lett.*, *22*, 1317–1320.

Lowman, J. P., S. D. King, and C. W. Gable (2001), The influence of tectonic plates on mantle convection patterns, temperature and heat flow, *Geophys. J. Int.*, *146*, 619–636.

Lowman, J., S. King, and C. Gable (2003), The role of the heating mode of the mantle in intermittent reorganization of the plate velocity field, *Geophys. J. Int.*, *152*, 455–467.

Minster, J. B., and T. H. Jordan (1978), Present day plate motions, *J. Geophys. Res.*, *83*, 5331–5354.

Mitrovica, J. X., and A. M. Forte (2004), A new inference of mantle viscosity based upon joint inversion of convection and glacial isostatic adjustment data, *Earth Planet. Sci. Lett.*, *225*, 177–189.

Monnereau, M., and S. Quéré (2001), Spherical shell models of mantle convection with tectonic plates, *Earth Planet. Sci. Lett.*, *184*, 575–587.

Nettelfield, D., and J. P. Lowman (2007), The influence of plate-like surface motion on upwelling dynamics in numerical mantle convection models, *Phys. Earth Planet. Int.*, *161*, 184–201.

Parmentier, E. M., C. Sotin, and B. J. Travis (1994), Turbulent 3-D thermal convection in an infinite Prandtl number, volumetrically heated fluid: Implications for mantle dynamics, *Geophys. J. Int.*, *116*, 241–251.

Quéré, S., and A. M. Forte (2006), Influence of past and present-day plate motions on spherical models of mantle convection: Implications for mantle plumes and hotspots, *Geophys. J. Int.*, *165*, 1041–1057.

Ratcliff, J. T., P. J. Tackley, G. Schubert, and A. Zebib (1997), Transitions in thermal convection with strongly variable viscosity, *Phys. Earth. Planet. Int.*, *102*, 201–212.

Ricard, Y., L. Fleitout, and C. Froidevaux (1984), Geoid heights and lithospheric stresses for a dynamic Earth, *Ann. Geophys.*, *2*, 267–286.

Richards, M. A., and B. H. Hager (1984), Geoid anomalies in a dynamic Earth, *J. Geophys. Res.*, *89*, 5987–6002.

Richards, M. A., and C. Lithgow-Bertelloni (1996), Plate motion changes, the Hawaiian-Emperor bend, and the apparent success and failure of geodynamical models, *Earth Planet. Sci. Lett.*, *137*, 19–27.

Richards, M. A., W.-S. Yang, J. Baumgardner, and H.-P. Bunge (2001), Role of a low-viscosity zone in stabilizing plate tectonics: Implications for comparitive terrestrial planetology, *Geochem. Geophys. Geosyst.*, *2*, 1026, doi:10.1029/2000GC000115.

Rona, P. A., and E. S. Richardson (1978), Early Cenozoic global plate reorganization, *Earth Planet. Sci. Lett.*, *40*, 1–11.

Sabadini, R., and D. A. Yuen (1989), Mantle stratification and long-term polar wander, *Nature*, *339*, 373–375.

Solomatov, V. S., and L.-N. Moresi (1997), Three regimes of mantle convection with non-Newtonian viscosity and stagnant lid convection on the terrestrial planets, *Geophys. Res. Lett.*, *24*, 1907–1910.

Spada, G., Y. Ricard, and R. Sabadini (1992), Excitation of true polar wander by subduction, *Nature*, *360*, 452–454.

Stacey, F. D. (1992), *Physics of the Earth*, 3rd ed., Brookfield Press, Brisbane, Queensland, Australia.

Stein, C., J. Schmalzl, and U. Hansen (2004), The effect of rheological parameters on plate behaviour in a self-consistent model of mantle convection, *Phys. Earth Planet. Int.*, *142*, 225–255.

Stock, J. M., and P. Molnar (1987), Revised history of the early Tertiary plate motion in the southwest Pacific, *Nature*, *325*, 495–499.

Tackley, P. J. (1998), Self-consistent generation of tectonic plates in three-dimensional mantle convection, *Earth Planet. Sci. Lett.*, *157*, 9–22.

Tackley, P. J. (2000a), Mantle convection and plate tectonics: Towards an integrated physical and chemical theory, *Science*, *288*, 2002–2007.

Tackley, P. J. (2000b), Self-consistent generation of tectonic plates in time-dependent, three-dimensional mantle convection simulations: 1. Pseudo-plastic yielding, *Geochem. Geophys. Geosyst.*, *1*, 1021, doi:10.1029/2000GC000036.

Tackley, P. J. (2000c), Self-consistent generation of tectonic plates in time-dependent, three-dimensional mantle convection simulations: 2. Strain weakening and asthenosphere, *Geochem. Geophys. Geosyst.*, *1*, 1026, doi:10.1029/2000GC000043.

Travis, B., and P. Olson (1994), Convection with internal heat sources and thermal turbulence in the Earth's mantle, *Geophys. J. Int.*, *118*, 1–19.

Travis, B., S. Weinstein, and P. Olson (1990a), Three-dimensional convection planforms with internal heat generation, *Geophys. Res. Lett.*, *17*, 243–246.

Travis, B., P. Olson, and G. Schubert (1990b), The transition from two-dimensional to three-dimensional planforms in infinite-Prandtl-number thermal convection, *J. Fluid Mech.*, *216*, 77–91.

Travis, B., C. J. Anderson, J. Baumgardner, C. W. Gable, B. H. Hager, R. J. O'Connell, P. Olson, A. Raefsky, and G. Schubert (1991), A benchmark comparison of numerical methods for infinite Prandtl number thermal convection in two-dimensional Cartesian geometry, *Geophys. Astrophys. Fluid. Dyn.*, *55*, 137–160.

Trompert, R., and U. Hansen (1998), Mantle convection simulations with rheologies that generate plate-like behaviour, *Nature*, *395*, 686–689.

Zhong, S., and M. Gurnis (1993), Dynamic feedback between a continent-like raft and thermal convection, *J. Geophys. Res.*, *98*, 12,219–12,232.

Zhong, S., and M. Gurnis (1995), Mantle convection with plates and mobile, faulted plate margins, *Science*, *267*, 838–843.

Zhong, S., M. T. Zuber, L. Moresi, and M. Gurnis (2000), Role of temperature-dependent viscosity and surface plates in spherical shell models of mantle convection, *J. Geophys. Res.*, *105*, 11,063–11,082.

C. W. Gable, Hydrology, Geochemistry, and Geology Group, EES-6, Los Alamos National Laboratory, Los Alamos, NM 87545, USA. (gable@lanl.gov)

A. D. Gait, School of Mathematics, University of Manchester, Oxford Road, Manchester M13 9PL, UK. (andrew.gait@manchester.ac.uk)

J. P. Lowman, Department of Physical and Environmental Sciences, University of Toronto Scarborough, 1265 Military Trail, Toronto, ON, Canada M1C 1A4. (lowman@utsc.utoronto.ca)